ARMY RESEARCH LABORATORY

A Geometrically Non-linear Model of Ceramic Crystals with Defects Applied to Silicon Carbide (SiC)

by John D. Clayton

ARL-TR-5096 **March 2010**

NOTICES

Disclaimers

The findings in this report are not to be construed as an official Department of the Army position unless so designated by other authorized documents.

Citation of manufacturer's or trade names does not constitute an official endorsement or approval of the use thereof.

Destroy this report when it is no longer needed. Do not return it to the originator.

Army Research Laboratory
Aberdeen Proving Ground, MD 21005-5066

ARL-TR-5096 **March 2010**

A Geometrically Non-linear Model of Ceramic Crystals with Defects Applied to Silicon Carbide (SiC)

John D. Clayton
Weapons and Materials Research Directorate, ARL

REPORT DOCUMENTATION PAGE	Form Approved OMB No. 0704-0188

1. REPORT DATE *(DD-MM-YYYY)*	2. REPORT TYPE	3. DATES COVERED (From - To)
March 2010	Final	January 2009-January 2010

4. TITLE AND SUBTITLE
A Geometrically Non-linear Model of Ceramic Crystals with Defects Applied to Silicon Carbide (SiC)

5a. CONTRACT NUMBER

5b. GRANT NUMBER

5c. PROGRAM ELEMENT NUMBER

6. AUTHOR(S)
John D. Clayton

5d. PROJECT NUMBER
AH80

5e. TASK NUMBER

5f. WORK UNIT NUMBER

7. PERFORMING ORGANIZATION NAME(S) AND ADDRESS(ES)
U.S. Army Research Laboratory
Terminal Effects Division
Weapons and Materials Research Directorate (ATTN: RDRL-WMP-B)
Aberdeen Proving Ground, MD 21005-5066

8. PERFORMING ORGANIZATION REPORT NUMBER
ARL-TR-5096

9. SPONSORING/MONITORING AGENCY NAME(S) AND ADDRESS(ES)

10. SPONSOR/MONITOR'S ACRONYM(S)

11. SPONSOR/MONITOR'S REPORT NUMBER(S)

12. DISTRIBUTION/AVAILABILITY STATEMENT
Approved for public release; distribution is unlimited.

13. SUPPLEMENTARY NOTES

14. ABSTRACT
A model is developed for anisotropic ceramic crystals undergoing potentially large deformations that can occur under significant pressures or high temperatures. The model is applied to enable an improved understanding of silicon carbide (SiC), with a focus on hexagonal polytype 6*H* of α-SiC. Incorporated in the model are the following features: non-linear anisotropic thermoelasticity, piezoelectricity and electrostriction, nucleation and glide of Shockley partial dislocations on the basal plane, dilatation from point defects and elastic fields of dislocation lines, and cleavage fracture. Physical properties are obtained from experimental data and calculations reported in the literature.

15. SUBJECT TERMS
Ceramic, defects, elasticity, plasticity, dielectric, piezoelectric, silicon carbide

16. SECURITY CLASSIFICATION OF:			17. LIMITATION OF ABSTRACT	18. NUMBER OF PAGES	19a. NAME OF RESPONSIBLE PERSON
a. REPORT	b. ABSTRACT	c. THIS PAGE	UU	24	John D. Clayton
Unclassified	Unclassified	Unclassified			19b. TELEPHONE NUMBER (*Include area code*) (410) 278-6146

Contents

List of Figures

List of Tables

1. Introduction

The crystal structure of silicon carbide (SiC) is dictated by its polytype. A SiC polytype is represented by the number of hexagonal planar SiC double layers in its unit cell, with an appended *C*, *H*, or *R* denoting a cubic, hexagonal, or rhombohedral structure. Over 200 structural polytypes of SiC single crystals are known to exist (Bernstein et al., 2005). Cubic polytypes are labeled β-SiC, while hexagonal and rhombohedral polytypes are labeled α-SiC. The common cubic (β) polytype is 3*C*-SiC, exhibiting the sphalerite or zinc blende crystal structure. Technologically relevant polytypes of hexagonal (α) SiC include 2*H* (wurtzite crystal structure), 4*H*, and 6*H*, while common rhombohedral polytypes include 9*R*, 12*R*, 15*R*, and 21*R*. Hexagonal polytype 6*H*-SiC is the focus of the present investigation; crystals of 6*H*-SiC are often referred to as moissanite. Polycrystalline structural ceramics, such as SiC-B and SiC-N are thought to consist primarily of 6*H*-SiC, though other polytypes may be present (Shih et al., 2000). Polytype 6*H*-SiC is non-centrosymmetric, piezoelectric, and spontaneously polar, i.e. pyroelectric (Qteish et al., 1993). Phase transformations at ambient temperatures are thought to occur at very high pressures on the order of 100 GPa (Vogler et al., 2006) though fractional increases of 6*H*-SiC grains relative to other polytypes have been observed to occur at somewhat lower compressive stresses (~19–32 GPa) in polycrystalline SiC subject to ballistic impact (Shih et al., 2000).

Defects can strongly affect mechanical, thermal, and electrical behaviors of ceramics, such as SiC. Basal slip of edge dislocations is thought to be the dominant mechanism of plastic deformation in hexagonal SiC polytypes, with dislocation mobility dependent on temperature and electric current (Galeckas et al., 2002). Shockley partial dislocations bordering intrinsic stacking faults are thought to be most relevant in hexagonal SiC (Samant et al., 1998; Blumeneau et al., 2003), with the mobility of leading partials exceeding that of trailing partials at low temperatures (Demenet et al., 2000) supporting a tendency for plasticity to be accompanied by generation of large numbers of stacking faults. Twinning, which is observed in β-SiC (Van Torne, 1966) does not appear to be an important deformation mechanism in hexagonal polytypes except under high temperatures and pressures wherein phase transformations occur. Point defects, such as Si and C vacancies (Shih et al., 2000; Bernstein et al., 2005) and interstitials, such as those generated by irradiation (Gao and Weber, 2005) may affect physical properties. Primary cleavage planes are of basal and prismatic orientations with single crystals of α-SiC apparently less resistant, in some cases, to fracture during indentation experiments than their polycrystalline counterparts (Kitahara et al., 2001) suggesting that cleavage of single crystals, in addition to grain boundary fracture, is important in failure assessment of polycrystals.

This report addresses the behavior of single crystals of 6*H*-SiC. A model incorporating coupled non-linear thermo-electro-mechanical behavior is developed in section 2 for proper interpretation

of results of shock physics experiments on anisotropic piezoelectric single crystals (Graham, 1972; Clayton, 2010). The primary content of this report consists, in section 3, of a number of tables of structural, mechanical, thermal, and electrical properties—either obtained from the open literature or newly computed—of hexagonal polytypes of SiC single crystals. Compression data for polycrystalline SiC has been reviewed extensively elsewhere (Dandekar, 2002).

The notation of non-linear continuum mechanics is used. The index notation follows the Einstein summation convention. Current configuration indices are written in lower case Latin, reference configuration indices in upper case Latin, and intermediate configuration indices in Greek. Superposed -1, *T*, and • denote the inverse, transpose, and material time derivative, respectively. Subscripted commas and semicolons denote partial and covariant differentiation, respectively.

2. General Model for Elastic Dielectrics with Defects

The framework of section 2 combines treatments of crystal plasticity of ceramic single crystals (Clayton, 2009a) and dielectrics with point defects (Clayton, 2009b) and may be applied to describe any single crystalline dielectric or semiconducting solid containing dislocations, stacking faults, and point defects. Let $x^a = x^a(X^A, t)$ denote spatial coordinates that depend on reference coordinates X^A of a material particle and time *t*. The deformation gradient in equations 1–3 is

$$F^{a}_{.A} = x^{a}_{,A} = F^{Ea}_{.\alpha}\bar{F}^{\alpha}_{.A} = F^{La}_{.\alpha}F^{P\alpha}_{.A}, \tag{1}$$

$$F^{La}_{.\alpha} = F^{Ea}_{.\alpha}\bar{J}^{1/3}, \tag{2}$$

$$\bar{F}^{\alpha}_{.A} = \bar{J}^{1/3}F^{P\alpha}_{.A}, \tag{3}$$

where

$F^{Ea}_{.\alpha}$: reversible thermoelastic deformation

$F^{P\alpha}_{.A}$: isochoric deformation from dislocation glide

$\bar{J}$: volume changes due to defects (Eshelby, 1954; Clayton, 2009a)

$F^{La}_{.\alpha}$: total lattice deformation

$\bar{F}^{\alpha}_{.A}$: total residual deformation

In equation 4, spatial velocity gradient $L^a_{.b}$ is

$$L^a_{.b} = v^a_{;b} = \dot{F}^{Ea}_{.\alpha} F^{E-1\alpha}_{.b} + F^{Ea}_{.\alpha} \bar{L}^{P\alpha}_{.\beta} F^{E-1\beta}_{.b} + \frac{1}{3} \dot{\overline{JJ}}^{-1} \delta^a_{.b} \tag{4}$$
$$= \dot{F}^{Ea}_{.\alpha} F^{E-1\alpha}_{.b} + F^{Ea}_{.\alpha} \left(\sum_i \dot{\gamma}^i \bar{s}^{i\alpha} \bar{m}^i_\beta \right) F^{E-1\alpha}_{.b} + \frac{1}{3} \dot{\overline{JJ}}^{-1} \delta^a_{.b},$$

where

$v^a = \dot{x}^a$: spatial velocity or particle velocity

$\bar{L}^{P\alpha}_{.\beta}$: plastic velocity gradient referred to the intermediate configuration

$\dot{\gamma}^i$: slip rate defined for each slip system *i*

$\bar{s}^{i\alpha}$: unit slip direction defined for each slip system *i*

$\bar{m}^i_\beta$: unit slip plane normal defined for each slip system *i*

$g_{ab} = \mathbf{g}_a \bullet \mathbf{g}_b$: spatial metric tensor

The metric tensor in the intermediate configuration is assumed Cartesian for simplicity, i.e., $g_{\alpha\beta} = \delta_{\alpha\beta}$.

In equations 5–8, Maxwell's equations in the quasi-electrostatic approximation (Maugin, 1988) for non-magnetic solids are written as

$$\varepsilon^{abc} \hat{e}_{c;b} = 0, \tag{5}$$

$$\frac{\partial \hat{d}^a}{\partial t} = -\hat{j}^a, \tag{6}$$

$$\hat{d}^a_{;a} = \hat{\rho}, \tag{7}$$

$$\hat{b}^a_{;a} = 0, \tag{8}$$

where

$\hat{e}_a = -\hat{\phi}_{,a} = -\hat{\phi}_{;a}$: spatial electric field

$\hat{d}^a = \varepsilon_0 \hat{e}^a + \hat{p}^a$: electric displacement

ε_0 : vacuum permittivity

$\hat{p}^a$: electric polarization per unit spatial volume

$\hat{j}^a = \hat{i}^a - (1/\mu_0) \varepsilon^{abc} \hat{b}_{c;b}$: effective electric (displacement) current density

$\hat{i}^a$: free electric current (vanishes in a perfect dielectric)

μ_0 : vacuum permeability

$\hat{\rho}$: free charge density per unit spatial volume (vanishes in a perfect dielectric)

$\hat{b}^a$: magnetic flux density

$\varepsilon^{abc} = \left[\sqrt{\det(g_{ab})} \right] e^{abc}$: = alternator tensor or permutation tensor

Partial time differentiation at fixed x^a is written $\partial / \partial t$. In equation 9, the total stress tensor is

$$T^{ab} = \sigma^{ab} + \hat{\tau}^{ab} = \sigma^{ab} + \hat{e}^a \hat{p}^b + \varepsilon_0 \hat{e}^a \hat{e}^b - \frac{\varepsilon_0}{2} \hat{e}^c \hat{e}_c g^{ab}, \tag{9}$$

where

σ^{ab} : mechanical Cauchy stress tensor

$\hat{\tau}^{ab}$: quasi-electrostatic Maxwell stress tensor

In equations 10–12, momentum balances and boundary conditions are

$$T^{ab}_{;b} + \bar{b}^a = \rho \dot{v}^a, \tag{10}$$

$$T^{ab} = T^{ba}, \tag{11}$$

$$\left[\!\left[T^{ab} \right]\!\right] n_b = T^{+ab} n_b - T^{-ab} n_b = 0, \tag{12}$$

where

$\bar{b}^a$: body force per unit spatial volume

ρ : spatial mass density

n_b : unit normal pointing from inside (–) to outside (+) of oriented surface element

In equations 13–14, the local balance of energy and entropy inequality are, respectively,

$$\rho \dot{e} = \sigma^{ab} L_{ab} + \hat{e}_a \dot{\hat{p}}^a - q^a_{;a} + \rho r, \tag{13}$$

$$\sigma^{ab} L_{ab} + \hat{e}_a \dot{\hat{p}}^a - \rho \dot{\psi} - \rho \dot{\theta} \eta - \frac{1}{\theta} \theta_{;a} q^a \geq 0, \tag{14}$$

where

e : internal energy per unit mass

q^a : heat flux (i.e., conduction)

r : heat source per unit mass (i.e., radiation)

$\psi = e - \theta\eta$: Helmholtz free energy per unit mass

θ : absolute temperature

η : entropy per unit mass

In equation 15, the free energy per unit mass is of the functional form

$$\psi = \psi\left(E^E_{\alpha\beta}, \overline{p}_\alpha, \theta, \xi, \varsigma, \vartheta\right), \tag{15}$$

where, in equations 16–17, the elastic strain tensor and intermediate polarization vector are, respectively,

$$E^E_{\alpha\beta} = \frac{1}{2}(C^E_{\alpha\beta} - \delta_{\alpha\beta}) = \frac{1}{2}(F^{Ea}{}_{.\alpha} g_{ab} F^{Eb}{}_{.\beta} - \delta_{\alpha\beta}), \tag{16}$$

$$\overline{p}_\alpha = F^{Ea}{}_{.\alpha} \hat{p}_a . \tag{17}$$

Also, ξ, ς, and ϑ are the scalar dislocation length per unit volume, stacking fault area per unit volume, and point defect concentration, respectively. In equations 18–21, constitutive relationships for stress, electric field, entropy, and heat flux consistent with equations 13 and 14 are

$$\overline{\Sigma}^{\alpha\beta} = J^E F^{E-1\alpha}{}_{.a} \sigma^{ab} F^{E-1\beta}{}_{.b} = \overline{\rho} \frac{\partial \psi}{\partial E^E_{\alpha\beta}} + J^E C^{E-1\alpha\chi} \overline{p}_\chi C^{E-1\beta\delta} \overline{e}_\delta , \tag{18}$$

$$\hat{e}^a = F^{Ea}{}_{.\alpha} \rho \frac{\partial \psi}{\partial \overline{p}_\alpha} = \rho \frac{\partial \psi}{\partial \hat{p}_a} , \tag{19}$$

$$\eta = -\frac{\partial \psi}{\partial \theta} , \tag{20}$$

$$\overline{q}^\alpha = -K^{\alpha\beta} \theta_{;\beta} , \tag{21}$$

where

$\overline{\rho} = \rho J^E = (\rho / 6) \varepsilon_{abc} \varepsilon^{\alpha\beta\chi} F^{Ea}{}_{.\alpha} F^{Eb}{}_{.\beta} F^{Ec}{}_{.\chi}$: intermediate mass density

$\overline{e}_\delta = F^{Ea}{}_{.\delta} \hat{e}_a = -F^{Ea}{}_{.\delta} \hat{\phi}_{;a}$: intermediate electric field

$\overline{q}^\alpha = J^E F^{E-1\alpha}{}_{.a} q^a$: intermediate heat flux

$\theta_{;\beta} = \theta_{;a} F^{Ea}{}_{.\beta}$: anholonomic temperature gradient

$K^{\alpha\beta}$: thermal conductivity

In equation 22, the Helmholtz free energy is written as follows on a per unit reference volume basis, where θ_0 is a reference temperature:

$$\begin{aligned}\rho_0\psi = &\frac{1}{2}C^{\alpha\beta\chi\delta}E^E_{\alpha\beta}E^E_{\chi\delta} + \frac{1}{6}C^{\alpha\beta\chi\delta\varepsilon\phi}E^E_{\alpha\beta}E^E_{\chi\delta}E^E_{\varepsilon\phi} \\ &+ \frac{1}{2}\Lambda^{\alpha\beta}\overline{p}_\alpha\overline{p}_\beta + \Delta^{\alpha\beta\chi}\overline{p}_\alpha E^E_{\beta\chi} + \frac{1}{2}\Upsilon^{\alpha\beta\chi\delta}\overline{p}_\alpha\overline{p}_\beta E^E_{\chi\delta} \\ &- \beta^{\alpha\beta}E^E_{\alpha\beta}(\theta-\theta_0) - \rho_0 c_V\theta\log\frac{\theta}{\theta_0} + \psi^R\left(\xi,\varsigma,\vartheta\right),\end{aligned} \tag{22}$$

where

$\rho_0 = \rho J = \rho J^E\overline{J} = (\rho/6)\varepsilon_{abc}\varepsilon^{ABC}F^a_{.A}F^b_{.B}F^c_{.C}$: reference mass density

Equations 23–31 apply for isothermal permittivity (i.e., dimensionless dielectric constants) $\varepsilon_{\alpha\beta}$, standard piezoelectric constants $e^{.\beta\chi}_{\alpha}$, pressure derivatives of dielectric constants at the reference state $\partial\varepsilon^{\alpha\beta}/\partial p$, second-order elastic constants at fixed electric field $C^{\alpha\beta\chi\delta}_{\bar{e}}$, thermal expansion coefficients at constant polarization $\alpha_{\alpha\beta}$, isobaric specific heat per unit mass c_p, Gruneisen numbers $\Gamma^{\alpha\beta}$ and Γ, and isothermal bulk modulus *B* (Polian et al., 1982):

$$\varepsilon_{\alpha\beta} = \delta_{\alpha\beta} + \varepsilon_0^{-1}\Lambda^{-1}_{\alpha\beta}, \tag{23}$$

$$e^{.\beta\chi}_{\alpha} = -\Lambda^{-1}_{\alpha\delta}\Delta^{\delta\beta\chi}, \tag{24}$$

$$\frac{\partial\varepsilon^{\alpha\beta}}{\partial p} = \frac{4}{3B\varepsilon_0}(\Upsilon^{\chi\delta\varepsilon}_{\ldots\varepsilon}\Lambda^{-1\alpha}_{\ .\chi}\Lambda^{-1\beta}_{\ .\delta} - \varepsilon_0\delta^{\alpha\beta} + \Lambda^{-1\alpha\beta}), \tag{25}$$

$$C^{\alpha\beta\chi\delta}_{\bar{e}} = C^{\alpha\beta\chi\delta} - \Delta^{\varepsilon\alpha\beta}\Lambda^{-1}_{\varepsilon\phi}\Delta^{\phi\chi\delta}, \tag{26}$$

$$\beta^{\alpha\beta} = C^{\alpha\beta\chi\delta}\alpha_{\chi\delta}, \tag{27}$$

$$c_p = c_V + (\alpha^{\beta}_{.\beta})^2\frac{B\theta}{\rho_0}, \tag{28}$$

$$\Gamma^{\alpha\beta} = \frac{\beta^{\alpha\beta}}{\rho_0 c_V}, \tag{29}$$

$$\Gamma = \frac{\alpha^{\beta}_{.\beta}B}{\rho_0 c_V}, \tag{30}$$

$$B = \frac{C_{33}(C_{11}+C_{12}) - 2(C_{13})^2}{C_{11}+C_{12}-4C_{13}+2C_{33}}. \tag{31}$$

Only two of the six possible coefficients of $\Upsilon^{\alpha\beta\chi\delta}$ are known from equation 25; it is assumed here for simplicity that $\Upsilon^{\alpha\beta\chi\delta} = \Upsilon^{\alpha\beta}\delta^{\chi\delta}$. Pyroelectricity is omitted in equation 22. Differences between isothermal and isentropic elastic coefficients are negligible in SiC near room temperature.

In equations 32–34, relevant dislocations in α-SiC include partial dislocations on the basal plane formed from the dissociation reaction $\frac{1}{3}[1\bar{2}10] \rightarrow \frac{1}{3}[1\bar{1}00] + \frac{1}{3}[0\bar{1}10]$ (Maeda et al., 1988; Samant et al., 1998; Demenet et al., 2000; Blumeneau et al., 2003). Dislocation kinetics are dictated by (Demenet et al., 2000):

$$\dot{\gamma}^i = A\left|\frac{\overline{\tau}^i}{\tau_C^i}\right|^{1/m} \exp\left(\frac{-Q}{\mathrm{k_B}\theta}\right)\mathrm{sgn}\left(\frac{\overline{\tau}^i}{\tau_C^i}\right), \tag{32}$$

$$\overline{\tau}^i = J^E \sigma^{ab} s_a^i m_b^i = C_{\alpha\chi}^E \overline{\Sigma}^{\chi\beta} \overline{s}^{i\alpha} \overline{m}_\beta^i, \tag{33}$$

$$m = \frac{\partial \log \overline{\tau}^i}{\partial \log \dot{\gamma}^i}, \tag{34}$$

where

A : a proportionality constant with dimensions of strain rate

Q : activation energy that may depend on electric current (Galeckas et al., 2002)

m : strain rate sensitivity

τ_C^i : intrinsic slip resistance or shear strength

In equation 35, residual elastic volume changes from screw dislocations are estimated as

$$\Delta V / V = \overline{J} - 1 \approx \frac{1}{\mu}\left(\frac{\partial \mu}{\partial p} - \frac{\mu}{B}\right) E_E \xi, \tag{35}$$

where

μ : effective elastic shear modulus

E_E : elastic energy per unit dislocation line length

Analogous formulae for edge dislocations and point defects are available in the literature (Eshelby, 1954; Holder and Granato, 1969; Clayton, 2009a; Clayton, 2010).

Table 1 lists parameters of the 6*H*-SiC crystal structure. The stacking sequence of Si or C layers in the [0001] direction (i.e., along the c-axis) is ABCACBABCACB…, meaning six hexagonal

planar layers each of Si and C comprise a single conventional unit cell. Tables 2 and 3 list fundamental and derived thermal, mechanical, and electrical properties of α-SiC. Material property tensors are expressed using Voigt's condensed notation. Tables 4–7 list properties and supporting references regarding defects and fracture. Predictions for volume changes associated with defects (see equation 35 and other equations in [Clayton, 2010]) are shown in figure 1.

Table 1. Structural features of 6*H*-SiC (room temperature and atmospheric pressure).

Parameter	**Value**	**Remarks**	**Reference**
a	0.308 nm	Lattice parameter (x^1-axis)	Stockmeier et al. (2009)
c	1.512 nm	Lattice parameter (x^3-axis)	
Ω_0	0.0103 nm^3	Atomic volume $\Omega_0 = \sqrt{3}a^2c/24$	
Point group	6*mm*	Dihexagonal pyramidal (HI)	Arlt and Schodder (1965)
Space group	C_{6v}^4 (*C*6*mc*)		Wyckoff (1963)

Table 2. Thermophysical properties (room temperature and atmospheric pressure).

Parameter	**Value**	**Remarks**	**Reference**
ρ_0	3210 kg/m^3	Mass density	Slack (1964)
c_p	652 J/kgK	Specific heat at constant pressure	Muller et al. (1998)
α_{11}	3.4×10^{-6} /K	Thermal expansion coefficients	Li and Bradt (1987)
α_{33}	3.2×10^{-6} /K		
β_{11}	2.3 MPa/K	Thermal stress coefficients	equation 27
β_{33}	2.1 MPa/K		
Γ_{11}	1.10	Gruneisen coefficients	equation 29
Γ_{33}	1.00		
Γ	1.06	Gruneisen parameter	equation 30
K_{11}	390 W/mK	Thermal conductivity	Burgemeister et al. (1979)
K_{33}	370 W/mK		
Θ_D	1200 K	Debye temperature	Slack (1964)
Θ_M	3375 K	Melting temperature	Merala et al. (1988)

Table 3. Elastic, piezoelectric, and dielectric properties (room temperature and atmospheric pressure).

Parameter	**Value**	**Remarks**	**Reference**
C_{11}	501 GPa	Second-order elastic constants; Brillouin scattering; 6*H*-SiC	Kamitani et al. (1997)
C_{12}	112 GPa		
C_{13}	52 GPa		
C_{33}	549 GPa		
C_{44}	161 GPa		
$\partial C_{11}/\partial p$	3.8	Pressure derivatives of second-order elastic coefficients; atomic model; 2*H*-SiC	Davydov (2004)
$\partial C_{12}/\partial p$	4.0		
$\partial C_{13}/\partial p$	4.0		
$\partial C_{33}/\partial p$	3.8		
$\partial C_{44}/\partial p$	-0.2		
μ	194 GPa	Isotropic elastic constants; Voigt averages; 6*H*-SiC	Blumeneau et al. (2003)
ν	0.161		
B	222 GPa		equation 31
B	230 GPa	Static compression; polycrystal	Bassett et al. (1993)
$\partial B/\partial p = B'$	4.0	Static compression; polycrystal	Bassett et al. (1993)
	3.1±0.3	Shock compression; polycrystal	Sekine and Kobayashi (1997)
	3.9	Isotropic elasticity, $\partial C_{\alpha\beta}/\partial p$	
	2.5	$\partial B/\partial p = 2\Gamma+1/3$	Slater (1939)
$\partial \mu/\partial p = \mu'$	3.4	Isotropic elasticity at fixed ν	
e_{15}	-0.198 C/m^2	Piezoelectric constants; atomic model; 6*H*-SiC	Mirgorodsky et al. (1995)
e_{31}	-0.200 C/m^2		
e_{33}	0.398 C/m^2		
ε_{11}	9.66	Static dielectric permittivity; experiment; 6*H*-SiC	Patrick and Choyke (1970)
ε_{33}	10.03		
$\partial \varepsilon_{11}/\partial p$	-0.0218 /GPa	Pressure derivatives of permittivity; DFT calculation; 4*H*-SiC	Karch et al. (1996)
$\partial \varepsilon_{33}/\partial p$	-0.0232 /GPa		
Λ_{11}	13.0 m/nF	Inverse dielectric susceptibilities	equation 23
Λ_{33}	12.5 m/nF		
Δ_{15}	2.58×10^9 C/(Fm)	Stress-polarization coefficients	equation 24
Δ_{31}	2.50×10^9 C/(Fm)		
Δ_{33}	-4.98×10^9 C/(Fm)		
Υ_{11}	-5.67 m/nF	Piezo-optic coefficients (electrostriction)	equation 25
Υ_{33}	-5.49 m/nF		

Table 4. Slip systems and Burgers vectors.

Type	**Direction**	**Plane**	**Burgers b**	**|*b*|**	**Planar spacing *d***
Basal, full	$<1\bar{2}10>$	(0001)	$1/3[1\bar{2}10]$	0.308 nm	0.252 nm (c/6)
Basal, partial	$<1\bar{1}00>$	(0001)	$1/3[1\bar{1}00]$	0.178 nm	0.252 nm (c/6)
Prism, full	$<1\bar{2}10>$	$\{10\bar{1}0\}$	$1/3[1\bar{2}10]$	0.308 nm	0.267 nm ($a\sqrt{3}/2$)

Table 5. Fracture properties.

Parameter	**Value**	**Plane**	**Remarks**	**Reference**
γ_F	8.6±0.4 J/m^2	(0001)	Cohesive energy; indentation experiment	Kitahara et al. (2001)
	5.6±0.5 J/m^2	$\{10\bar{1}0\}$		
	4.0±0.2 J/m^2	$\{\bar{1}2\bar{1}0\}$		
τ_F	37.7 GPa	(0001)	Theoretical strength $\tau_F = \frac{\mu b}{2\pi d}$	Frenkel (1926)
	35.6 GPa	$\{10\bar{1}0\}$		

Table 6. Dislocation properties (unless noted otherwise: basal dislocations, ~room temperature).

Parameter	**Value**	**Defect type**	**Remarks**	**Reference**
E_E	21.1 nJ/m	Full 60°	Elastic energy; isotropic	Blumeneau et al. (2003)
	6.1 nJ/m	Partial 30°	Elastic energy; anisotropic	
	7.2 nJ/m	Partial 90°	Elastic energy; anisotropic	
	18.5 nJ/m	Edge loop	Elastic energy; isotropic	
E_C	0.72 nJ/m	Partial 30° (Si)	Core energy; DFT; 2*H*-SiC	Blumeneau et al. (2003)
	0.74 nJ/m	Partial 90° (Si)	Core energy; DFT; 2*H*-SiC	
	1.25 nJ/m	Partial 30° (C)	Core energy; DFT; 2*H*-SiC	
	1.81 nJ/m	Partial 90° (C)	Core energy; DFT; 2*H*-SiC	
W_{SF}	2.5±0.9 mJ/m^2	(0001) plane	Stacking fault energy; ~1800K	Maeda et al. (1988)
τ_C	4.5 GPa	Unknown	Shock; polycrystal @ HEL	Feng et al. (1998)
	3.3±1.0 GPa	Unknown	Shock; polycrystal above HEL	Vogler et al. (2006)
	6.8 GPa	Unknown	Static compression; polycrystal	Zhang et al. (2002)
	4.5±0.4 GPa	Unknown	Indentation; single crystal	Shim et al. (2008)
	0.45 GPa	Partial basal	Static compression; 823 K	Samant et al. (1998)
	4.3 GPa	Full basal	Numerical; single crystal	Zhang et al. (2005)
	7.5 GPa	Full prism	Numerical; single crystal	Zhang et al. (2005)
	0.014 GPa	Partial basal	Theory; $\tau_C = W_{SF}/b$	Maeda et al. (1988)

Table 6. Dislocation properties (unless noted otherwise: basal dislocations, ~room temperature). (continued)

Parameter	Value	Defect type	Remarks	Reference
τ_P	1.24 GPa	Full basal 60°	Theory; Peierls-Nabarro stress $\tau_P = 2\hat{K}\exp\left(\frac{-2\pi\hat{K}d}{\mu b}\right)$; $\frac{\hat{K}}{\mu}\sim 1$	Nabarro (1947)
	0.060 GPa	Partial 30°		
	0.014 GPa	Partial 90°		
	0.70 GPa	Full prism edge		
m	3.0±0.7	Partial basal	Rate sensitivity of yield stress	Samant et al. (1998)
Q	2.5 eV	Partial basal	Activation energy; null bias	Samant et al. (1998)
	0.27 eV	Partial basal	Activation energy; $\hat{j}$=0.5A/cm^2	Galeckas et al. (2002)

Table 7. Point defect properties.

Parameter	Value	Type	Remarks	Reference
E_F	3.4 eV	C	Vacancy formation energy	Bernstein et al. (2005)
	5.3 eV	Si		
$\delta\Omega$	-0.0066 nm^3	C	Relaxation volume (infinite medium)	Eshelby (1954)
	-0.0082 nm^3	Si	$\delta\Omega = -[3\Omega_0 E_F/(2\mu)]^{1/2}$	

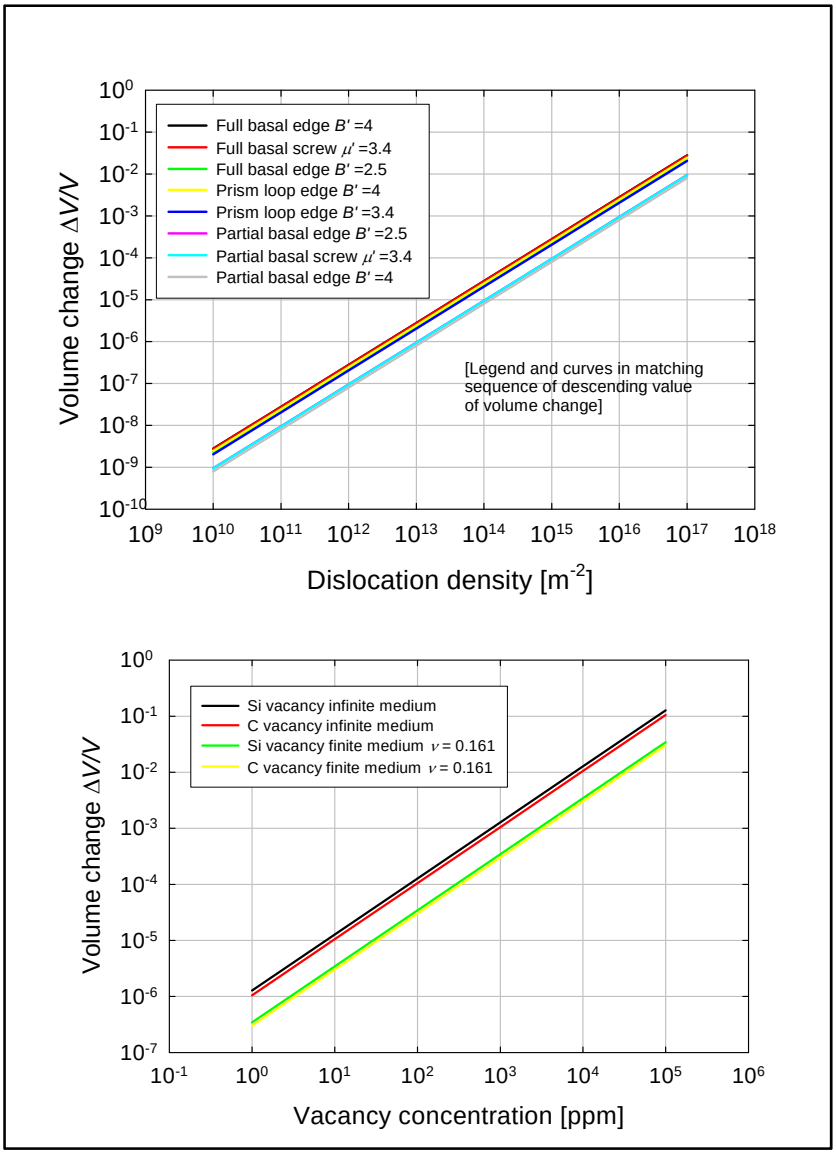

Figure 1. Predicted volume changes from dislocations and vacancies in α-SiC.

4. Conclusions

A non-linear continuum theory has been developed for modeling the coupled electromechanical behavior of anisotropic elastic-plastic ceramic single crystals with defects. Governing equations and thermodynamic definitions of physical properties have been derived and concisely presented. Comprehensive tables of compiled (from values in the literature) and computed physical properties of 6*H*-SiC have been presented to serve as reference material to support future meso-scale modeling efforts of ceramic material systems.

5. References

Arlt, G.; Schodder, G. Some elastic constants of silicon carbide. *J. Acoustic Soc. Amer*. **1965**, *37*, 384–386.

Bassett, W. A.; Weathers, M. S.; Wu, T. C.; Holmquist, T. Compressibility of SiC up to 68.4 GPa. *J. Appl. Phys*. **1993**, *74*, 3824–3826.

Bernstein, N.; Gotsis, H. J.; Papaconstantopoulos, D. A.; Mehl, M. J. Tight-binding calculations of the band structure and total energies of the various polytypes of silicon carbide. *Phys. Rev. B.* **2005**, *71*, 075203.

Blumeneau, A. T.; Fall, C. J.; Jones, R.; Oberg, S.; Frauenheim, T.; Briddon, P. R. Structure and motion of basal dislocations in silicon carbide. *Phys. Rev. B.* **2003**, *68*, 174108.

Burgemeister, E. A.; Von Muench, W.; Pettenpaul, E. Thermal conductivity and electrical properties of 6H silicon carbide. *J. Appl. Phys*. **1979**, *50*, 5790–5794.

Clayton, J. D. A continuum description of nonlinear elasticity, slip and twinning, with application to sapphire. *Proc. R. Soc. Lond. A.* **2009a**. *465*, 307–334.

Clayton, J. D. A non-linear model for elastic dielectric crystals with mobile vacancies. *Int. J. Non-Linear Mech*. **2009b**, *44*, 675–688.

Clayton, J. D. Modeling nonlinear electromechanical behavior of shocked silicon carbide. *J. Applied Phys*. **2010**, *107*, 013520.

Dandekar, D. P. *A Survey of Compression Studies on Silicon Carbide (SiC)*; ARL-TR-2695; U.S. Army Research Laboratory: Aberdeen Proving Ground, MD, 2002.

Davydov, S. Y. Effect of pressure on the elastic properties of silicon carbide. *Phys. Sol. State.* **2004**, *46*, 1200–1205.

Demenet, J. L.; Hong, M. H.; Pirouz, P. Plastic behavior of 4H-SiC single crystals deformed at low strain rates. *Scripta Mater*. **2000**, *43*, 865–870.

Eshelby, J. D. Distortion of a crystal caused by point imperfections. *J. Appl. Phys*. **1954**. *25*, 255–261.

Feng, R.; Raiser, G. F.; Gupta, Y. M. Material strength and inelastic deformation of silicon carbide under shock wave compression. *J. Appl. Phys*.**1998**, *83*, 79–86.

Frenkel, J. Zur theorie der elastizitasgrenze und der festigkeit kristallinscher korper. *Z. Phys.* **1926**, *37*, 572–609.

Galeckas, A.; Linnros, J.; Pirouz, P. Recombination-enhanced extension of stacking faults in 4H-SiC p-i-n diodes under forward bias. *Appl. Phys. Lett*. **2002**, *81*, 883–885.

Gao, F.; Weber, W. J. Atomic-level computer simulation of SiC: defect accumulation, mechanical properties and defect recovery. *Phil. Mag*. **2005**, *85*, 509–518.

Graham, R. A. Strain dependence of longitudinal piezoelectric, elastic, and dielectric constants of X-cut quartz. *Phys. Rev. B.* **1972**, *6*, 4779–4793.

Holder, J.; Granato, A. V. Thermodynamic properties of solids containing defects. *Phys. Rev*. **1969**, *182*, 729–741.

Kamitani, K.; Grimsditch, M.; Nipko, J. C.; Loong, C. K. The elastic constants of silicon carbide: a Brillouin-scattering study of 4H and 6H SiC single crystals. *J. Appl. Phys*. **1997**, *82*, 3152–3154.

Karch, K.; Bechstedt, F.; Pavone, P.; Strauch, D. Pressure-dependent properties of SiC polytypes. *Phys. Rev. B.* **1996**, *53*, 13400–13413.

Kitahara, H.; Noda, Y.; Yoshida, F.; Nakashima, H.; Shinohara, N.; Abe, H. Mechanical behavior of single crystalline and polycrystalline silicon carbides evaluated by Vickers indentation. *J. Cer. Soc. Japan*. **2001**, *109*, 606–606.

Li, Z.; Bradt, R. C. Thermal expansion and thermal expansion anisotropy of SiC polytypes. *J. Amer. Soc*. **1987**, *70*, 445–448.

Maeda, K.; Suzuki, S.; Fujita, M.; Ishihara, M.; Hyodo, S. Defects in plastically deformed 6H SiC single crystals studied by transmission electron microscopy. *Phil. Mag. A.* **1988**, *57*, 573–592.

Maugin, G. A. *Continuum Mechanics of Electromagnetic Solids*; North-Holland: Amsterdam, 1988.

Merala, T. B.; Chan, H. W.; Howitt, D. G. Dislocation microstructures in explosively deformed hard materials. *Mater. Sci. Eng. A.* **1988**, *105–106*, 293–298.

Mirgorodsky, A. P.; Smirnov, M. B. Abdelmounim, E.; Merle, T.; Quintard, P. E. Molecular approach to the modeling of elasticity and piezoelectricity of SiC polytypes. *Phys. Rev. B.* **1995**, *52*, 3993-4000.

Muller, S. G.; Eckstein, R.; Fricke, J.; Hofmann, D.; Hofmann, R.; Horn, R.; Mehling, N.; Nilsson, O. Experimental and theoretical analysis of the high temperature thermal conductivity of monocrystalline SiC. *Mater. Sci. Forum*. **1998**, *264–268*, 623–626.

Nabarro, F.R.N. Dislocations in a simple cubic lattice. *Proc. Phys. Soc*. **1947**, *59*, 256–272.

Patrick, L.; Choyke, J. Static dielectric constant of SiC. *Phys. Rev. B.* **1970**, *2*, 2255–2256.

Polian, A.; Besson, J. M.; Grimsditch, M.; Vogt, H. Elastic properties of GaS under high pressure by Brillouin scattering. *Phys. Rev. B.* **1982**, *25*, 2767–2775.

Qteish, A.; Heine, V.; Needs, R. J. Structural and electronic properties of SiC polytypes. *Physica B.* **1993**, *185*, 366–378.

Samant, A. V.; Zhou, W. L.; Pirouz, P. Effect of test temperature and strain rate on the yield stress of monocrystalline 6H-SiC. *Phys. Stat. Solidi A.* **1998**. *166*, 155–169.

Sekine, T.; Kobayashi, T. Shock compression of 6H polytype SiC to 160 GPa. *Phys. Rev. B.* **1997**. *55*, 8034–8037.

Shih, C. H.; Meyers, M. A.; Nesterenko, V. F.; Chen, S. J. Damage evolution in dynamic deformation of silicon carbide. *Acta Mater*. **2000**, 48, 2399–2420.

Shim, S.; Jang, J.; Pharr, G. M. Extraction of flow properties of single-crystal silicon carbide by nanoindentation and finite element simulation. *Acta Mater*. **2008**, *56*, 3824–3832.

Slack, G. A. Thermal conductivity of pure and impure silicon, silicon carbide, and diamond. *J. Appl. Phys*. **1964**, *35*, 3460–3466.

Slater, J. C. *Introduction to Chemical Physics*; McGraw-Hill: New York, 1939.

Stockmeier, M.; Muller. R.; Sakwe, S. A.; Wellmann, P. J.; Magerl, A. On the lattice parameters of silicon carbide. J. *Appl. Phys*. **2009**, *105*, 033511.

Van Torne, L. I. Twinning in β-silicon carbide. *Phys. Stat. Solidi*, **1966**, *14*, K123–K126.

Vogler, T. J.; Reinhart, W. D.; Chhabildas, L. C.; Dandekar, D. P. Hugoniot and strength behavior of silicon carbide. *J. Appl. Phys*. **2006**, *99*, 023512.

Wyckoff, R.W.G. *Crystal Structures*; John Wiley and Sons: New York, 1963.

Zhang, J.; Wang, L.; Weidner, D. J.; Uchida, T.; Xu, J. The strength of moissanite. *Amer. Mineralogist*. **2002**, *87*, 1005–1008.

Zhang, D.; Wu, M. S.; Feng, R. Micromechanical investigation of heterogeneous microplasticity in ceramics deformed under high confining stress. *Mech. Mater*. **2005**, *37*, 95–112.

No. of Copies	Organization
1 (PDF only)	DEFENSE TECHNICAL INFORMATION CTR DTIC OCA 8725 JOHN J KINGMAN RD STE 0944 FORT BELVOIR VA 22060-6218
1	DIRECTOR US ARMY RESEARCH LAB IMNE ALC HRR 2800 POWDER MILL RD ADELPHI MD 20783-1197
1	DIRECTOR US ARMY RESEARCH LAB RDRL CIM L 2800 POWDER MILL RD ADELPHI MD 20783-1197
1	DIRECTOR US ARMY RESEARCH LAB RDRL CIM P 2800 POWDER MILL RD ADELPHI MD 20783-1197
	ABERDEEN PROVING GROUND
33	DIR USARL RDRL CIM G (BLDG 4600) RDRL WMP B S BILYK D CASEM J CLAYTON (15 COPIES) D DANDEKAR M GREENFIELD C HOPPEL J HOUSKAMP Y HUANG R KRAFT B LEAVY B LOVE M RAFTENBERG M SCHEIDLER T WEERASOORIYA C WILLIAMS RDRL WMP C T BJERKE RDRL WMP F N GNIAZDOWSKI RDRL WMP H C MEYER

INTENTIONALLY LEFT BLANK.